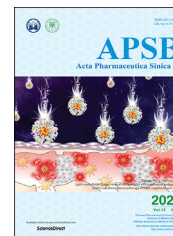




Chinese Pharmaceutical Association  
Institute of Materia Medica, Chinese Academy of Medical Sciences

Acta Pharmaceutica Sinica B

[www.elsevier.com/locate/apsb](http://www.elsevier.com/locate/apsb)  
[www.sciencedirect.com](http://www.sciencedirect.com)



ORIGINAL ARTICLE

# Enhanced uptake and anti-maturation effect of celastrol-loaded mannosylated liposomes on dendritic cells for psoriasis treatment



Long Xi<sup>a</sup>, Zibei Lin<sup>a</sup>, Fen Qiu<sup>a</sup>, Shaokui Chen<sup>a</sup>, Ping Li<sup>b</sup>, Xin Chen<sup>a</sup>,  
Zhenping Wang<sup>c</sup>, Ying Zheng<sup>a,\*</sup>

<sup>a</sup>State Key Laboratory of Quality Research in Chinese Medicine, Institute of Chinese Medical Sciences, University of Macau, Macau 999078, China

<sup>b</sup>Beijing Hospital of Traditional Chinese Medicine, Affiliated with Capital Medical University, Beijing 100050, China

<sup>c</sup>Department of Dermatology, School of Medicine, University of California, San Diego, CA 92093, USA

Received 15 March 2021; received in revised form 5 May 2021; accepted 11 June 2021

## KEY WORDS

Psoriasis;  
Celastrol;  
Mannose;  
Liposome;  
Anti-maturation;  
Dendritic cells;  
Microneedle;  
Inflammation

**Abstract** Psoriasis is an autoimmune skin disease in which dendritic cells (DCs) trigger the progression of psoriasis by complex interactions with keratinocytes and other immune cells. In the present study, we aimed to load celastrol, an anti-inflammatory ingredient isolated from Chinese herbs, on mannosylated liposomes to enhance DC uptake as well as to induce DC tolerance in an imiquimod-induced psoriasis-like mouse model. Mannose was grafted onto liposomes to target mannose receptors on DCs. The results demonstrated that compared with unmodified liposomes, DCs preferred to take up more fluorescence-labeled mannosylated liposomes. After loading celastrol into mannose-modified liposomes, they effectively inhibited the expression of maturation markers, including CD80, CD86 and MHC-II, on DCs both *in vitro* and *in vivo*. Additionally, after intradermal injection with a microneedle, celastrol-loaded mannose-modified liposomes (CEL-MAN-LPs) achieved a superior therapeutic effect compared with free drug and celastrol-loaded unmodified liposomes in the psoriasis mouse model in terms of the psoriasis area and severity index, histology evaluation, spleen weight, and expression of inflammatory cytokines. In conclusion, our results clearly revealed that CEL-MAN-LPs was an effective formulation for psoriasis treatment and suggested that this treatment has the potential to be applied to other inflammatory diseases triggered by activated DCs.

\*Corresponding author. Tel.: +853 88224687; fax: +853 28841358.

E-mail address: [yzheng@umac.mo](mailto:yzheng@umac.mo) (Ying Zheng).

Peer review under responsibility of Chinese Pharmaceutical Association and Institute of Materia Medica, Chinese Academy of Medical Sciences.

<https://doi.org/10.1016/j.apsb.2021.07.019>

2211-3835 © 2022 Chinese Pharmaceutical Association and Institute of Materia Medica, Chinese Academy of Medical Sciences. Production and hosting by Elsevier B.V. This is an open access article under the CC BY-NC-ND license (<http://creativecommons.org/licenses/by-nc-nd/4.0/>).

## 1. Introduction

Psoriasis is a chronic, autoimmune skin disease that affects approximately 125 million people globally<sup>1</sup>. Visible changes in appearance, including erythema, scaling, and thickening on the skin lesions of psoriasis patients lead to psychological problems in their social lives<sup>2</sup>. Moreover, psoriasis is also associated with other comorbidities, such as psoriatic arthritis<sup>3</sup> and cardiovascular disease<sup>4</sup>. At present, the mechanism of psoriasis is still unclear. It is generally known that environmental stimuli, genetic factors, and medications can trigger the pathogenesis of psoriasis<sup>5</sup>. As an autoimmune disease, psoriasis shows disorders in both innate and acquired immunity, where dendritic cells (DCs) act as professional antigen-presenting cells<sup>6,7</sup>. During the progression of psoriasis, mature myeloid DCs present antigens to naïve T cells with MHC molecules and activate naïve T cells through costimulatory molecules such as CD 80 and CD 86. Meanwhile, innate immune cytokines, IL-12, IL-23 and tumor necrosis factor alpha (TNF- $\alpha$ ), are secreted by DCs to stimulate the activities of crucial T cell populations and the hyperproliferation of keratinocytes<sup>8–10</sup>. Recent studies have demonstrated that inhibiting the activation of DCs achieved good antipsoriasis efficacy<sup>11,12</sup>.

*Tripterygium wilfordii* Hook F. which is a traditional Chinese herbal medicine has been widely utilized to treat inflammatory diseases, including rheumatoid arthritis, systemic lupus erythematosus, and psoriasis for many years<sup>13,14</sup>. Celastrol (CEL), a pentacyclic triterpenoid compound extracted from *T. wilfordii* Hook F, demonstrated anti-inflammatory and antioxidant potential in inflammatory diseases<sup>15,16</sup>. Additionally, a recent study showed that CEL could inhibit DC activation and subsequently suppress T cell responses<sup>17</sup>. However, as a small molecule drug with a low target-specific ability to DCs, CEL may have restricted therapeutic efficacy.

Recently, surface-specificity modified nanoparticles, which can be recognized by receptors on the surface of DCs, have been utilized in cancer and inflammation therapeutics<sup>18,19</sup>. These drug delivery systems have shown good potential to improve DC uptake, subsequently inducing DC maturation or leading to DC tolerance<sup>19–21</sup>. Moreover, the cellular uptake mediated by receptors on DCs can cause active agents to be specifically delivered to dendritic cells, thus reducing immune-related adverse side effects. Mannose receptors that are highly expressed on DCs are desirable targets for receptor-mediated delivery strategies<sup>22–24</sup>. Mannosylated polymeric carriers have been applied in some anti-inflammatory therapies, and impressive progress has been made<sup>25,26</sup>. DC dysfunction is essential in the pathogenesis of psoriasis. However, to the best of our knowledge, the DC targeting strategy has not been applied in psoriasis therapy.

Approximately 80%–90% of psoriasis patients suffer from mild to moderate disease, which affects less than 20% of the body surface<sup>27,28</sup>. For this situation, topical treatment is highly recommended because of its low systemic exposure and targeting ability on the skin lesion<sup>29</sup>. However, effective delivery of nanoparticles to the epidermis or dermis must overcome the firm stratum corneum barriers. Recently, microneedle technology has attracted increasing attention to increase the skin permeability of nanoparticles. As a microinvasive method, the micron-sized needle-like structure can

painlessly deliver the active agent across the stratum corneum, only creating reversible microchannels with proper patient compliance<sup>30,31</sup>. Various microneedles, such as solid microneedles, coated microneedles, hollow microneedles and dissolvable microneedles, have been designed for different purposes<sup>32–35</sup>. Compared with other types of microneedles, hollow microneedles can infuse a massive amount of drug into the dermis layer<sup>36</sup>. MicronJet600, a marketed hollow microneedle device, has been used in immunotherapy and insulin administration<sup>37,38</sup>.

In this study, to enhance the target-specific ability of celastrol to DCs, we prepared CEL-loaded mannose-modified liposomes (CEL-MAN-LPs) and explored the mannose receptor-mediated uptake of fluorescence-labeled mannosylated liposomes by dendritic cells both *in vitro* and *in vivo*. Then, the anti-maturation activity of CEL-MAN-LPs on DCs was tested *in vitro* on bone marrow-derived DCs. Finally, we intradermally injected CEL-MAN-LPs into imiquimod (IMQ)-induced psoriasis-like mice with hollow microneedles and further evaluated the therapeutic effect and antipsoriasis mechanism of CEL-MAN-LPs. This study reported for the first time that the mannosylated drug delivery system enhanced the uptake and anti-maturation efficacy of active agents on DCs in psoriasis therapy.

## 2. Materials and methods

### 2.1. Materials

CEL was obtained from Chengdu Pufei De Biotech Co., Ltd. (Chengdu, China). Lecithin and Tween 80 were purchased from Aladdin Industrial Corporation (Shanghai, China). 1,2-Distearoyl-*sn*-glycero-3-phosphoethanolamine-*N*-[methoxy (polyethylene glycol-2000)]-mannose (mannose-PEG2000-DSPE) was synthesized by Shanghai Toyang Biotech Inc. (Shanghai, China). Methanol and chloroform were purchased from Damao Chemical Reagent Factory (Tianjin, China). IMQ was purchased as Aldara, a topical cream (5% imiquimod; Health Care Limited, Loughborough, UK). Hair remover spray foam (Linco Care Ltd., Manchester, UK) was purchased from Sasa (Macau, China). Recombinant mouse GM-CSF (554586), recombinant mouse IL-4 (550067), PE-Cy7-conjugated anti-mouse CD45 (552848) and PerCP-Cy5.5-conjugated anti-mouse I-A/I-E (562363) were purchased from BD Biosciences (San Diego, CA, USA). Fetal bovine serum (FBS), APC-conjugated anti-mouse CD11c (17-0114-82), FITC-conjugated anti-mouse CD80 (11-0801-82) and PE-conjugated anti-mouse CD86 (12-0862-82) were purchased from Thermo Fisher Scientific (Waltham, MA, USA). Mouse IL-23 ELISA Kits (433704) were purchased from Biolegend (San Diego, CA, USA). Anti-IL-23 antibody (ab45420), anti-Ki-67 antibody (ab15580), anti-IL-17A antibody (ab79056), Alexa Fluor® 488-conjugated goat anti-rabbit IgG H&L (ab150077) and goat anti-rabbit IgG H&L (Biotin) (ab6720) were obtained from Abcam (Cambridge, UK). HRP-conjugated streptavidin (SE068) and 3,3'-diaminobenzidine (DA1010) were obtained from Beijing Solarbio Science & Technology Co., Ltd. (Beijing, China). 3,3'-Diiodoacetylcarbocyanine perchlorate (DiO), 1,1'-diiodoacetyl-3,3,3',3'-tetramethylindocarbocyanine (DiI) and Hoechst 33342

were purchased from Invitrogen (Carlsbad, CA, USA). DNase I (10104159001) was purchased from Roche Molecular Biochemicals (Rotkreuz, Switzerland). Collagenase type IV (LS004188) and collagenase type II (LS004176) were purchased from Worthington Biochemical Corp. (New Jersey, USA). Milli-Q water was obtained from a Millipore Direct-Q ultrapure water system (Millipore, Bedford, USA).

## 2.2. Animals and cell lines

C57/BL6 mice (female, 6–8 weeks old), which were reared under specific pathogen-free conditions, were obtained from the Faculty of Health Sciences of the University of Macau. All animal studies were conducted following the NIH Guidelines for the Care and Use of Laboratory Animals, and the animal experimental protocols were approved by the University of Macau Animal Ethics Committee.

The JAWS II cell line was obtained from American Type Culture Collection (ATCC, USA). The cells were cultured with alpha MEM (Gibco,  $\alpha$ -MEM, nucleosides, 12571-063) containing 10% (*v/v*) FBS, 100 U/mL penicillin–streptomycin, and 20 ng/mL murine GM-CSF at 37 °C under 5% CO<sub>2</sub>.

## 2.3. Hollow microneedle devices

The hollow microneedle device (MicronJet600, NanoPass Technologies Ltd., Nes Ziona, Israel) used in our study is composed of three 600  $\mu$ m-length silicon microneedles bonded to the tip of a plastic hub, which can be installed to a standard Luer syringe.

## 2.4. Preparation of CEL-MAN-LPs

In this study, CEL-MAN-LPs were prepared using a thin-film dispersion method. Briefly, CEL, lecithin, Tween 80, and mannose-PEG2000-DSPE at a weight ratio of 2:70:15:15, 2:70:15:10, 2:70:15:5 or 2:85:15:0 were dissolved in chloroform in a flask to prepare CEL-MAN-LPs or CEL-LPs, respectively. After that, the chloroform was removed with a rotary evaporator at 40 °C under a vacuum of 200 Mbar to generate a thin layer on the flask, and then the dried lipid layer was hydrated using 0.9% saline at 50 °C for 40 min with spinning. The suspension was collected and sonicated using a probe ultrasound device (37.5 W, 3 mm probe, 2 s/2 s) for 4 min. To generate a uniform particle size distribution, the preparations were passed through a polycarbonate membrane with a pore size of 100 nm using a mini-extruder (Avestin, LF-1, Canada) 20 times.

## 2.5. Characterization of CEL-MAN-LPs

The size distribution and zeta potential of the CEL-MAN-LPs were measured using dynamic light scattering (DLS) (Malvern, Worcestershire, WR, UK). Before the test, the samples were diluted five times with 0.9% saline. Each sample was tested three times. The stability of CEL-MAN-LPs was evaluated with DLS at 4 °C for up to 3 months.

To calculate the encapsulation of the CEL-MAN-LPs, free CEL was separated with ultrafiltration. In brief, the solution of CEL-MAN-LPs was centrifuged at 4000 rpm (Heraeus™ Multifuge™ X3R, Thermo Fisher Scientific, Waltham, MA, USA) for 60 min in an ultrafiltration tube (3-kDa cutoff). The total amount of CEL in the CEL-MAN-LP solution before centrifugation and the amount of free CEL in the filtrate were detected with HPLC.

For the HPLC method, the test was conducted using an Agilent 1200 series system (Agilent, USA) with a C18 column (Agilent Zorbax; 4.6 mm  $\times$  250 mm, 5  $\mu$ m) at room temperature. HPLC elution was conducted with methanol–0.4% H<sub>3</sub>PO<sub>4</sub> solution (85:15, *v/v*) at a rate of 1 mL/min. The sample volume was 10  $\mu$ L, and the wavelength of the UV detector was set at 430 nm. After detection, the following equations were used to calculate the encapsulation efficiency [EE (%)] and drug-loading capacity [DLC (%)]:

$$EE (\%) = \frac{\text{Total drug} - \text{Free drug}}{\text{Total drug}} \times 100 \quad (1)$$

$$DLC (\%) = \frac{\text{Drug}}{\text{Drug} + \text{Carrier agent}} \times 100 \quad (2)$$

The *in vitro* drug release profile of CEL and CEL-MAN-LPs was investigated as previously described with some modification<sup>39</sup>. Briefly, CEL-MAN-LPs containing 200  $\mu$ g of CEL were suspended in 1 mL of PBS and transferred into a dialysis bag (MWCO 8000–14,000 Da). Then, the dialysis bag was placed in 50 mL of 1% Tween 80 solution (*w/v*) (in 1  $\times$  PBS) and shaken in the dark at 120 rpm. The release medium (1 mL) was sampled and replaced with fresh buffer at the same volume after 2, 4, 8, 10, 12, 24, 36 and 48 h. The cumulative release amount of CEL was detected with HPLC as described above. The release profile of CEL was studied with the same method. Before the test, CEL was solubilized in a mixed solution containing Cremophor EL, ethanol and H<sub>2</sub>O (1:1:10, *v/v/v*).

To detect the morphology of the CEL-MAN-LPs, the CEL-MAN-LPs were negatively stained with 2% (*w/v*) neutral phosphotungstic acid and observed under transmission electron microscopy (TEM, JEM-2100F, Tokyo, Japan) at an accelerating voltage of 80 kV. For the concanavalin A (CON A) agglutination assay, Con A solution (1  $\mu$ mol/L) was added to 0.5 mg/mL liposomes. TEM was used to observe the aggregated CEL-MAN-LPs. The particle size distribution was measured by DLS.

## 2.6. In vitro DC uptake

JAWS II DCs were seeded in a 12-well plate at a density of 1  $\times$  10<sup>5</sup> cells/well and incubated with DiI-LPs (0.8  $\mu$ g/mL), 5% (mannose-PEG2000-DSPE/total carrier, *w/w*) DiI-MAN-LPs, 10% DiI-MAN-LPs, and 15% DiI-MAN-LPs for 4 h at 37 °C with 5% CO<sub>2</sub>. In investigation experiments of mannose receptor-mediated uptake, 20 mg/mL D-mannose was added 30 min prior to the treatment of liposomes. The cellular uptake of DiI by JAWS II cells was measured with flow cytometry (BD LSRFortessa, BD, USA).

In the qualitative analysis, DiI-LPs (5  $\mu$ g/mL) and 15% DiI-MAN-LPs were used to treat JAWS II cells (1  $\times$  10<sup>5</sup> cells/well) for 2, 4 and 8 h at 37 °C with 5% CO<sub>2</sub>, and then the nuclei were stained with Hoechst 33258 (Invitrogen, USA). Confocal laser scanning microscopy (TCS SP8II, Leica, Germany) was used to visualize the fluorescence of DiI in JAWS II cells.

## 2.7. Isolation and culture of mouse BMDCs

C57/BL mice (male, 7–9 weeks of age) were sacrificed by inhalation of CO<sub>2</sub>. The mouse femurs and tibias were removed under sterile conditions. The ends of the bones were cut off, and the bone marrow was rinsed out from the bone cavity with 2% FBS-PBS and collected into a sterile centrifuge tube. After

centrifugation at 1000 rpm (Heraeus™ Multifuge™ X3R, Thermo Fisher Scientific, Waltham, MA, USA) for 5 min, the supernatant was discarded. The pellet was lysed with red blood cell lysis buffer for 3 min. The BMDCs were washed with 2% FBS-PBS and resuspended in RPMI 1640 medium containing 10% FBS, 100 U/mL penicillin/streptomycin, 20 ng/mL GM-CSF and 20 ng/mL IL-4. BMDCs ( $1 \times 10^6$  cell/mL) were seeded in six-well plates and cultured in an incubator at 37 °C with 5% CO<sub>2</sub>. Half of the medium was replaced every other day. On Day 6, immature BMDCs were collected by gentle agitation with a pipette for the next experiments.

#### 2.8. Anti-maturation effect of the CEL-MAN-LPs on BMDCs *in vitro*

Immature BMDCs were isolated and cultured according to section 2.7. Free CEL (25 ng/mL), CEL-LPs and CEL-MAN-LPs were used to pretreat immature BMDCs ( $5 \times 10^5$  cell/well) in nontissue culture-treated 96-well U-bottom plates for 4 h. After that, R848 (1 µg/mL) was applied to induce the maturation of BMDCs in an incubator at 37 °C with 5% CO<sub>2</sub>. After 24 h, the levels of IL-23 in the supernatants were measured using IL-23 ELISA kits. The BMDCs were collected and incubated with diluted anti-CD11c, anti-CD80, anti-CD86 and anti-I-A/I-E antibodies for 20 min at 4 °C to detect the maturation status of BMDCs with flow cytometry (BD LSRFortessa, BD, USA).

#### 2.9. DC uptake of the MAN-LPs in mice

The *in vivo* DC uptake test was performed on the IMQ-induced psoriasis mouse model (model establishment is described in section 2.10). After applying IMQ for 6 days, 50 µL of DiO-LPs (187.5 µg/kg) and DiO-MAN-LPs were intradermally injected into the top, middle and bottom site of the back skin with hollow microneedles, respectively. The vertical distance between each injection site was about 1.5 cm. The mice were sacrificed after 4 and 24 h. The full-thickness skin and draining lymph nodes (DLNs, axillary, brachial and inguinal lymph nodes) were harvested to prepare a single-cell suspension. Briefly, the DLNs were ground and passed through 70-µm cell screens, and the isolated cells were dispersed in 1% FBS-PBS. For the skin samples, the full-thickness skin was minced with scissors and digested with 2.5 mg/mL collagenase type II, 2.5 mg/mL collagenase type IV, and 0.5 mg/mL DNase I in PBS containing 1% BSA at 37 °C under continuous stirring for 90 min, after which the samples were quenched with DMEM containing 10% FBS and passed through a 70-µm cell mesh. To mark DCs in a single-cell suspension, isolated cells were stained with anti-CD45 and anti-CD11c antibodies. The DiO fluorescence taken by the DCs of the skin and DLNs was measured with flow cytometry (BD LSRFortessa, BD, USA).

#### 2.10. Topical administration in an IMQ-induced psoriasis-like mouse model

The IMQ-induced psoriasis-like mouse model was established according to our previous studies<sup>29</sup>. Briefly, IMQ cream (62.5 mg containing 3.125 mg of the active ingredient) was applied to the shaved back skin of female C57/BL mice for 6 days. For the *in vivo* dosing regimen, after receiving imiquimod cream for 4 h, the mice received an intradermal injection of 50 µL of 0.9% saline (IMQ group), CEL solution (375 µg/kg), CEL-LPs and CEL-MAN-LPs on three different points of the back skin using

MicronJet600 hollow microneedles for 6 days. The injection sites were chosen according to section 2.9. On Day 7, the mice were sacrificed. Full-thickness skin, skin DLNs, and spleen samples were taken for experiments.

#### 2.11. Psoriasis area and severity index (PASI) scores evaluation

The PASI scores were used to measure the severity of psoriasis skin lesions. The factors in this scoring system include erythema and desquamation on a scale of 0–4, as follows: 0, none; 1, mild; 2, moderate; 3, severe; and 4, very severe. The scoring was conducted independently by two people daily for 7 days. The overall score of the factors reflects the severity of inflammation on a scale of 0–8.

#### 2.12. Weight ratio of spleen to body (spleen/body, %, w/w)

The spleen is an important lymphoid organ of the human body and is a storage site for immune cells such as B cells and T cells. Splenomegaly is a typical phenomenon of inflammation<sup>40</sup>. The spleen/body (% w/w) is an evaluation index of the severity of inflammation. After the mice were sacrificed, the spleens were harvested, and the spleen/body (% w/w) was immediately measured, avoiding water loss of the samples.

#### 2.13. Histological analysis

The back skin was collected at the end of the experiment and fixed with 4% paraformaldehyde, subsequently embedded in paraffin. After dewaxing and hydration, 4-µm-thick sections were stained with hematoxylin and eosin (H&E), and then observed with a microscope (BDS 200, Aote, China) at 400 × magnification.

#### 2.14. Immunohistochemistry (IHC) and immunofluorescence (IF) staining

For IHC staining, the paraffin sections were first deparaffinized and hydrated, and then the sections were treated with 3% hydrogen peroxide for 10 min at room temperature. After blocking nonspecific antigens, the sections were incubated with primary antibodies, including anti-IL17 antibody (1:100 dilution) and anti-IL-23 antibody (1:100 dilution), overnight at 4 °C. After that, the sections were incubated with biotin-linked secondary antibody (1:500 dilution) for 1 h followed by incubation with HRP-conjugated streptavidin (1:100 dilution) for 30 min. Finally, 3,3'-diaminobenzidine was used for chromogenic detection, and the stained sections were counterstained with hematoxylin. Images of the sections were captured with a microscope (BDS 200, Aote, China) at 400 × magnification. For the IHC quantification, the staining intensity of IL-17 and IL-23 in 3 random visual fields of the skin sample was calculated with ImageJ software.

For IF staining, the skin samples were embedded in OCT. Samples were sectioned into 10-µm sections. The sections were fixed in 4% paraformaldehyde for 15 min at room temperature and then washed in PBS. For staining the intracellular protein, permeabilization and blocking procedures were performed with 10% goat serum containing 0.3% Triton X-100 for 60 min at room temperature. Primary antibodies (Ki67, 1:200 dilution) were incubated overnight at 4 °C in 10% goat serum containing 0.3% Triton X-100. Sections were rinsed with PBS and incubated with Alexa Fluor® 488-conjugated secondary antibodies (1:500 dilution) for 1 h at room temperature. The slides were mounted with

ProLong Gold Antifade Mountant with DAPI and observed with confocal laser scanning microscopy (TCS SP8II, Leica, Germany). The fluorescent intensity of Ki67 in the epidermis of the skin sample was quantified with ImageJ software.

### 2.15. Quantification of mRNA by real-time PCR (qRT-PCR)

The back skin sample (50 mg) was added to 500  $\mu$ L of TRIzol reagent (Invitrogen, USA) and homogenized with the TissueLysor II System (Qiagen, CA, USA) at 30 frequency/s for 10 min to extract total mRNA. The reverse transcription was performed with the PrimeScript RT Reagent Kit (Takara, Japan) on a C1000 Touch thermal cycler system (Bio-Rad, UK) according to the manuscript protocol. The reaction cycle was 37  $^{\circ}$ C for 15 min, 85  $^{\circ}$ C for 5 s and kept at 4  $^{\circ}$ C. qRT-PCR was conducted with SYBR Premix Ex Taq II (Takara, Japan) on a VIIA7 Real-Time PCR instrument (Applied Biosystems, USA), following the manufacturer's instructions. The primer sequences are listed in Table 1. The comparative Ct method ( $\Delta\Delta$ Ct) was used to calculate the relative mRNA levels.

### 2.16. Evaluation of the maturation state of the DCs in the lymphoid organs

To detect the maturation state of DCs, the spleen and lymph nodes were ground and passed through 70- $\mu$ m cell screens to prepare single-cell suspensions, and the isolated cells were dispersed in 1% FBS-PBS. After blocking FcR, the single-cell suspensions were incubated with anti-mouse CD45, anti-mouse I-A/I-E, anti-mouse CD11c, anti-mouse CD80 and anti-mouse CD86 antibodies for 20 min at 4  $^{\circ}$ C in the dark. Isotype antibodies were used as negative controls. Acquisition was performed by flow cytometry (BD LSRFortessa, BD, USA).

### 2.17. Safety evaluation of CEL-MAN-LPs on the skin of healthy mice

To test the skin safety of the treatment, 50  $\mu$ L of 0.9% saline, CEL solution (375  $\mu$ g/kg), CEL-LPs or CEL-MAN-LPs were injected on three different sites of the mouse back skin with hollow microneedles for 6 days. The selection of the injection site referred to section 2.9. To evaluate the status of the skin, the images of the back skin were recorded on Days 1, 4 and 7.

**Table 1** Primer sequences of mouse genes examined by quantitative real-time PCR.

Primer	Base sequence (5' to 3')
<i>Il-1<math>\beta</math></i> (S)	CCCTGCAGCTGGAGAGTGTGGA
<i>Il-1<math>\beta</math></i> (AS)	TGTGCTCTGCTTGTGAGGTGCTG
<i>Il-6</i> (S)	CCTCTCTGCAAGAGACTTCCAT
<i>Il-6</i> (AS)	AGTCTCCTCTCCGGACTTGT
<i>Il-17A</i> (S)	TTAACTCCCTTGGCGCAAAA
<i>Il-17A</i> (AS)	CTTTCCTCCGCATTGACAC
<i>Il-23</i> (S)	TCCTCCAGCCAGAGGATCACCC
<i>Il-23</i> (AS)	AGAGTTGCTGCTCCGTGGGG
<i>Tnf-<math>\alpha</math></i> (S)	GCCCACGTCGTAGCAAACCAC
<i>Tnf-<math>\alpha</math></i> (AS)	GCAGGGGCTCTTGACGGCAG
<i>Gapdh</i> (S)	GGGCTCTCTGCTCCTCCTGT
<i>Gapdh</i> (AS)	CGGCCAAATCCGTTACACCCG

### 2.18. Statistical analysis

The statistical significance of the differences between different groups was determined via one-way ANOVA, where  $P < 0.05$  was considered as statistically significant difference.

## 3. Results and discussion

### 3.1. Preparation and characterization of CEL-MAN-LPs

As shown in Fig. 1A, the hydrodynamic size of CEL-MAN-LPs (15% mannose lipid grafted ratio) was  $85.5 \pm 0.7$  nm with a PDI of  $0.248 \pm 0.01$ , indicating a homogenous particle size distribution. TEM imaging (Fig. 1A) shows that CEL-MAN-LPs had a regular spherical shape without visible aggregation. After storage at 4  $^{\circ}$ C for 3 months, the particle size of CEL-MAN-LPs did not significantly change, indicative of satisfactory stability (Fig. 1B). The free drug was removed using a hyperfiltration tube, and the EE (%) and DLC (%) were detected with HPLC. The results showed that the EE (%) and DLC (%) of CEL in CEL-MAN-LPs were  $90.8 \pm 0.4\%$  and  $1.78 \pm 0.01\%$ , respectively, indicating effective CEL loading. For the *in vitro* cumulative drug release (Fig. 1C), CEL-MAN-LPs showed a sustained release profile where only approximately 35% of CEL released after incubation in the release medium for 48 h. In contrast, the solubilized CEL released much faster than CEL-MAN-LPs. Nearly 80% of CEL released into the medium after 12 h. After being modified with different grafted ratios of mannose-PEG2000-DSPE, the particle size of the LPs increased with the mannose lipid grafted ratios from  $75.0 \pm 0.7$  nm to  $85.5 \pm 0.7$  nm (Fig. 1D), and the zeta potential of the LPs decreased with the mannose lipid grafted ratios from  $-1.8 \pm 0.2$  to  $-6.0 \pm 0.3$  (Fig. 1E). To further confirm whether mannose-PEG2000-DSPE was effectively grafted onto the liposomes, the agglutination efficiency was evaluated as described in the previous reports<sup>41</sup>. CONA, a plant lectin, specifically binds to terminal  $\alpha$ -D-mannosyl, causing aggregation of mannose-modified nanoparticles. The TEM image shows that the CEL-MAN-LPs formed larger aggregates after addition of CONA (Supporting Information Fig. S1). Moreover, the DLS results are shown in Fig. 1F and G. As expected, for the CEL-MAN-LPs, the particle size and PDI significantly increased after incubation with CONA. However, the CEL-LPs barely changed in particle size and PDI, indicating that mannose was successfully grafted onto the liposome surface.

### 3.2. In vitro cellular uptake evaluation

To evaluate the effect of the mannose lipid-grafted ratio on DC uptake, JAWS II cells were incubated with unmodified DiI-LPs and DiI-MAN-LPs at different grafting ratios. The DiI fluorescence intensity in the cells was quantified with flow cytometry. After incubating for 4 h, the amount of DiI uptake by DCs in all the mannose-grafted LP groups was markedly higher than that in the ungrafted LP group (Fig. 2A and B). Moreover, the uptake by DCs increased with the mannose lipid grafting ratio. Specifically, when the grafted ratio of mannose lipid reached 15%, the DiI uptake in the DiI-MAN-LPs group was more than two times higher than that in the DiI-LPs group, suggesting effective DC uptake of mannose lipid-grafted liposomes. However, when we further increased the grafted ratio of the mannose lipid to 20%, the liposomes demonstrated a broad particle size distribution. So 15%

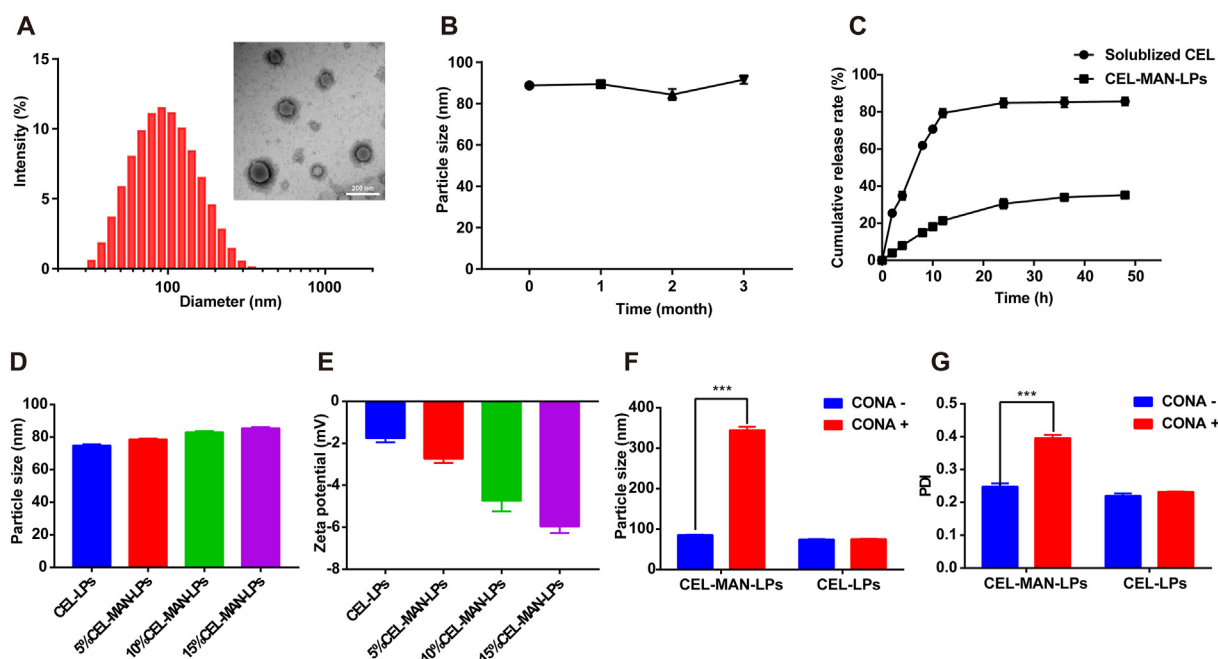


**Figure 1** Characterization of CEL-MAN-LPs. (A) Particle size profile and TEM image of CEL-MAN-LPs. (B) The stability of CEL-MAN-LPs at 4 °C for 3 months analyzed by DLS. (C) *In vitro* drug release profile of CEL-MAN-LPs and solubilized CEL in PBS (pH 7.4) with 1% Tween 80. (D) The particle size and (E) Zeta potential of CEL-MAN-LPs with different grafted ratios of mannose-PEG2000-DSPE. (F) Particle size and (G) PDI changes of CEL-MAN-LPs and CEL-LPs before and after adding CONA solution. Data points shown are mean  $\pm$  SD ( $n = 3$ ), \*\*\* $P < 0.001$ , compared with the indicated group. Scale bar = 200 nm.

was considered to be a proper grafted ratio of the mannose lipid. To investigate whether the enhanced uptake by DCs was mediated by the mannose receptor, as the competitor of the mannose receptor, free D-mannose was used to pretreat JAWS II cells. The results of flow cytometry quantification shown in Fig. 2C demonstrate that the uptake of DiI-MAN-LPs by DCs was markedly reduced after pretreatment with D-mannose compared with the control group. Based on these results, we can conclude that this mannose modification strategy could enhance DC uptake *via* mediation of the mannose receptor. To further evaluate DC uptake, the localization of DiI fluorescence in JAWS II cells was visualized with confocal microscopy. As shown in Fig. 2D and E, the fluorescence intensity located in the DCs in the 15% DiI-MAN-LP group was significantly higher than that in the DiI-LP group at different incubation time points (*i.e.*, 2, 4, and 8 h), consistent with the flow cytometry results (Fig. 2B). As the MAN-LPs with a 15% mannose lipid grafted ratio showed excellent delivery efficiency, this optimized formulation was selected for further *in vivo* mouse studies.

### 3.3. CEL-MAN-LPs inhibited the maturation of BMDCs *in vitro*

DCs are a type of innate immune cell that plays a vital role in the pathological process of psoriasis. Mature myeloid DCs release inflammatory cytokines and stimulate T cells, subsequently triggering the development of psoriasis<sup>1</sup>. The costimulatory molecules on the surface of mature DCs, such as CD80, CD86 and MHC-II, are essential for activating T cells. Since the therapeutic targets of CEL-MAN-LPs are myeloid DCs, we attempted to test the anti-inflammatory effect of CEL preparations on BMDCs *in vitro*. R848, a TLR7/8 agonist, was used here to establish an inflammatory DC model. As shown in Supporting Information Fig. S2, the purity of the cultured BMDCs was more than 85%, indicating successful isolation of the BMDCs. The CEL could

inhibit the expression of costimulatory molecules (CD80 and CD86) on the BMDCs which were induced with R848, and the anti-maturation ability of CEL was dose-dependent with concentration (Supporting Information Fig. S3). We further investigated the anti-maturation effect of CEL preparations. For cytokine detection, the IL-23 level in the supernatant of the BMDCs was dramatically increased after induction with R848. Moreover, as shown in Fig. 3A, CEL, CEL-LPs and CEL-MAN-LPs significantly inhibited the secretion of IL-23. The effect on the maturation status of the DCs is shown in Fig. 3B–D where R848 successfully induced the expression of CD80, CD86 and MHC-II on the BMDCs. Meanwhile, the expression of these maturation markers was significantly decreased after pretreatment with CEL, CEL-LPs and CEL-MAN-LPs, and the blank vehicle showed no effect on the maturation status of BMDCs. Notably, the anti-maturation efficacy of CEL was obviously enhanced by encapsulation into the MAN-LPs. The above results may be because the mannose modification strategy could markedly increase DC uptake of CEL and then showed a better anti-maturation effect on DCs, which was further tested in section 3.4.

### 3.4. DC uptake in the skin and DLNs of mice

In psoriatic skin lesions in mice, a certain number of myeloid DCs accumulate in the dermis as antigen-presenting cells and trigger the immune response. The skin DLNs are secondary lymphoid organs, where the nanoparticles and drugs can be drained to the DLNs through the lymphatic vessels after penetrating the dermis layer<sup>42</sup>. To effectively deliver the DiO-MAN-LPs to the dermis, we applied the hollow microneedles. Because the DiO-MAN-LPs mainly accumulated in the stratum corneum without the hollow microneedles (Supporting Information Fig. S4). In this study, following intradermal injection of DiO-MAN-LPs and DiO-LPs with hollow microneedles, DCs were isolated from skin and DLN samples, and the ratios of DiO-positive DCs were

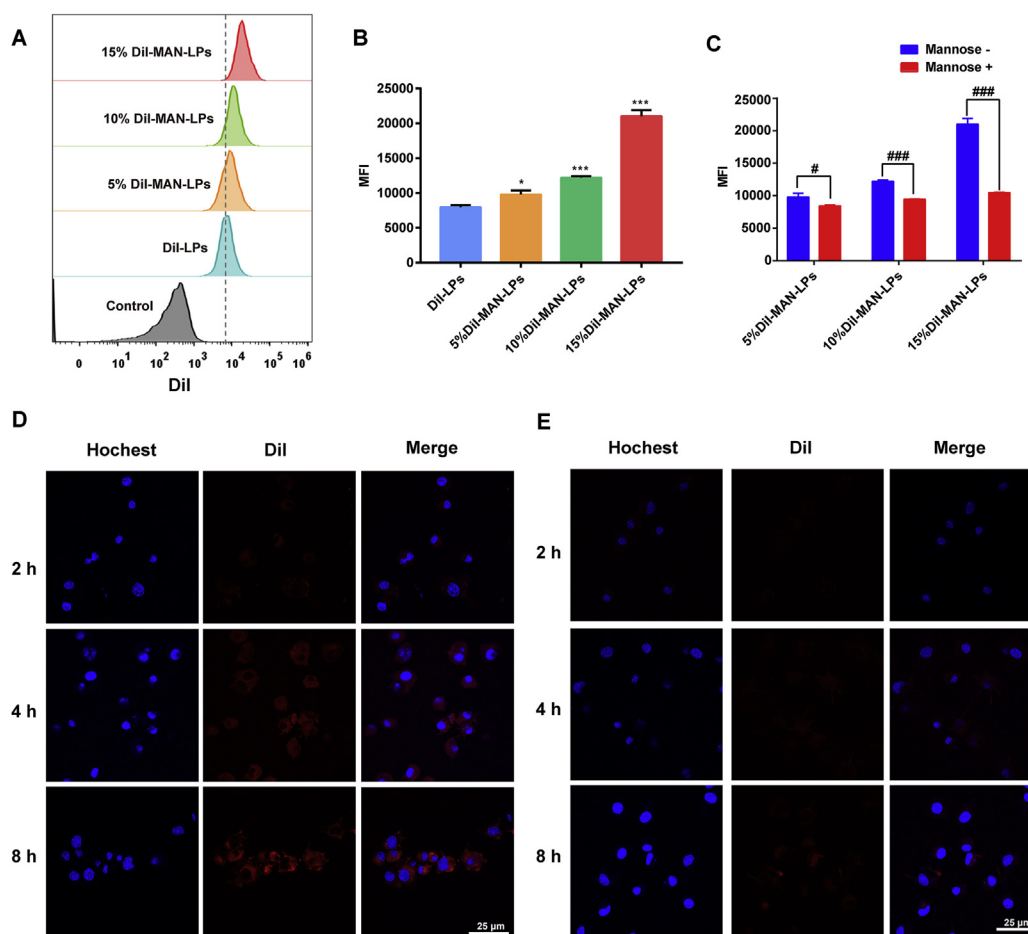


**Figure 2** *In vitro* uptake of MAN-LPs and LPs by JAWS II cells. (A) Histogram profiles and (B) mean fluorescence intensity analyzed by flow cytometry after incubation with DiI-MAN-LPs (different grafted ratio) and DiI-LPs for 4 h. (C) The intracellular uptake of DiI-MAN-LPs (different grafted ratio) after being pretreated with or without mannose. Confocal images to show uptake of (D) 15% DiI-MAN-LPs and (E) DiI-LPs after incubation for 2, 4 and 8 h. Nuclei (blue), DiI (red). Data are represented as mean value  $\pm$  SD ( $n = 3$ ), where  $*P < 0.05$ ,  $***P < 0.001$  compared with DiI-LPs group.  $#P < 0.05$ ,  $##P < 0.01$ ,  $###P < 0.001$  compared with indicated group. Scale bar = 25  $\mu$ m.

determined with flow cytometry. The gating strategy is illustrated in Supporting Information Fig. S5. As shown in Fig. 4, after administrating the preparations for 4 and 24 h, the ratios of DiO-positive DCs from the skin and DLN samples in the DiO-MAN-LPs group were markedly higher than those in the DiO-LPs group, indicating that the mannose modification strategy can enhance DC uptake of LPs in the psoriasis mouse model.

### 3.5. Histology evaluation

Photographs of psoriatic skin lesions in different groups are demonstrated in Fig. 5. Compared with the normal mice, psoriasis pathological symptoms such as white scale, red skin and thickened skin were obviously observed on the back skin of the mice in the IMQ-induced group (Fig. 5B). The symptoms of white scales and erythema on skin lesions were relieved after treatment with free CEL, CEL-LPs and CEL-MAN-LPs. Moreover, the back skin of the mice treated with CEL-MAN-LPs showed the slightest pathological symptoms. The H&E results were consistent with the appearance of the skin lesion (Fig. 5C). A single layer of basal cells was observed in the epidermis of the normal mice, but hyperplasia of basal cells displaying a multilayered arrangement was observed in IMQ-induced mouse skin (Fig. 5D). CEL-LPs, CEL-

MAN-LPs and CEL inhibited the hyperplasia of epidermal cells. Among all the tested groups, the CEL-MAN-LPs showed the best bioactivity.

### 3.6. PASI evaluation

The degrees of erythema and desquamation on the psoriatic mouse back skin were scored for 7 days and are summarized in Fig. 6. The symptoms of desquamation and erythema started to be exhibited on the skin lesion on Day 2 and were increased with time during the treatment, and the degree of the pathological symptoms reached a peak on Day 6 and slightly declined on Day 7. For the CEL group, the symptoms of desquamation were mitigated significantly ( $P < 0.001$ ) compared with those in the IMQ only group (Fig. 6B), but no significant changes were observed in the severity of erythema, suggesting a limited therapeutic effect on psoriatic skin (Fig. 6A). For CEL-LPs and CEL-MAN-LPs, the scores of desquamation, erythema and total PASI were significantly lower than those in the IMQ group (Fig. 6A–C). Moreover, the CEL-MAN-LP group had the lowest PASI scores among all the therapeutic groups after 6 days of treatment, reflecting its excellent antipsoriasis activity.

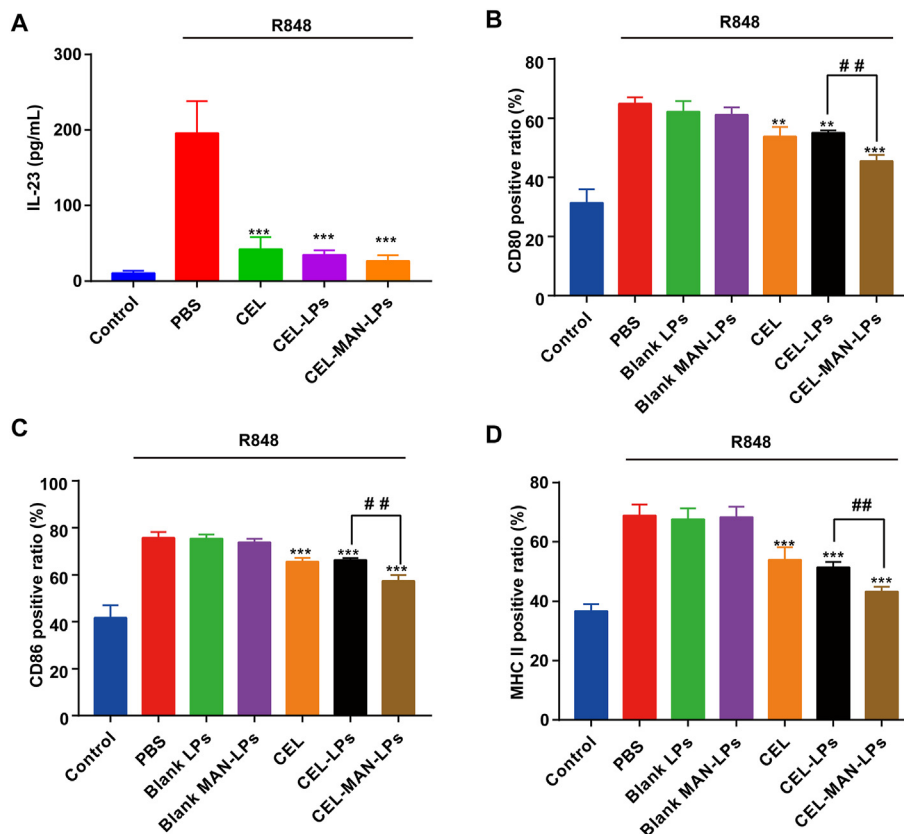


**Figure 3** The anti-maturation effect of CEL-MAN-LPs on BMDCs. (A) The protein levels of IL-23 in the supernatant. (B) CD 80, (C) CD 86 and (D) MHC-II expression on BMDCs after being pretreated with CEL (25 ng/mL), CEL-MAN-LPs, CEL-LPs, blank MAN-LPs, blank LPs for 4 h and subsequently induced with R848 for 24 h. Data are represented as mean  $\pm$  SD ( $n = 4$ ). \*\* $P < 0.01$ , \*\*\* $P < 0.001$ , compared with R848 group. ## $P < 0.01$ , compared with indicated group.

### 3.7. CEL-MAN-LPs mitigated splenomegaly in a mouse model

As shown in Fig. 6D, serious splenomegaly was caused by application of IMQ on the mouse dorsal skin for 6 days, where the spleen/body (% *w/w*) of the IMQ group was almost three times higher than that of the normal group. The spleen/body (% *w/w*) of all the therapeutic groups showed a decreasing trend compared with the psoriasis model group. However, there were no statistically significant differences in the CEL and CEL-LP groups at the

0.05 level. Notably, CEL-MAN-LPs significantly reduced the inflammation-induced splenomegaly ( $P < 0.01$ ).

### 3.8. CEL-MAN-LPs suppressed the mRNA expression of inflammatory cytokines in psoriatic skin lesions

The expression levels of inflammatory cytokines in psoriatic skin are closely related to the severity and therapeutic index of psoriasis. As shown in Fig. 7, the mRNA expression levels of *Il-*

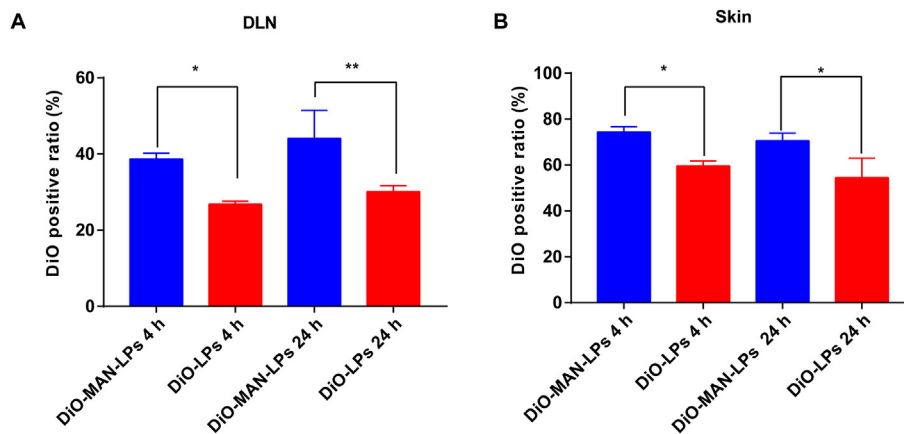


**Figure 4** *In-vivo* DC uptake of DiO-MAN-LPs and DiO-LPs in mice skin and DLN. DC uptake in (A) DLN and (B) skin after intradermally delivering DiO-MAN-LPs and DiO-LPs with hollow microneedles for 4 and 24 h, respectively. Data are represented as mean  $\pm$  SD ( $n = 3$ ). \* $P < 0.05$ , \*\* $P < 0.01$ , by comparison with indicated groups.

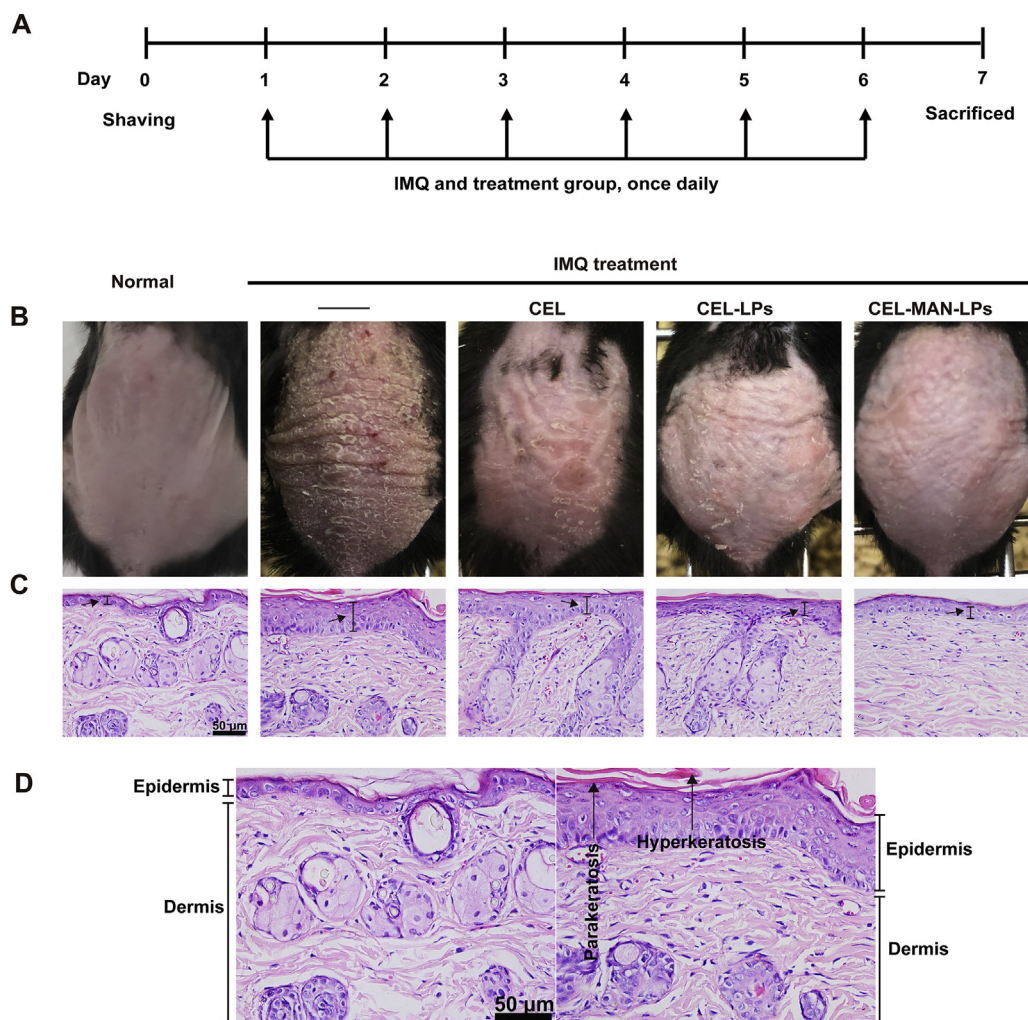


**Figure 5** Psoriatic symptom of the skin lesion after topical application of IMQ and intradermal injection of different preparations. (A) The timeline of the experiment. (B) The photographs of the dorsal skin of mice were taken on Day 7. (C) The H&E staining ( $\times 400$ ) was conducted to observe histological changes in skin lesions of mice after the treatment with CEL, CEL-LPs and CEL-MAN-LPs. (D) Enlarged view of H&E sections of normal mice group (left) and the IMQ (right). Scale bar = 50  $\mu\text{m}$ .

$Il-1\beta$ ,  $Il-6$ ,  $Il-17A$ ,  $Il-23$  and  $Tnf-\alpha$  in IMQ-induced skin were dramatically upregulated compared with those in the normal control group. After the treatment of mice with CEL-LPs and CEL-MAN-LPs, the mRNA levels of  $Il-1\beta$ ,  $Il-6$ ,  $Il-17A$ ,  $Il-23$  and  $Tnf-\alpha$  in the affected skin were dramatically inhibited. Comparatively, in the CEL group, only the mRNA levels of  $Il-1\beta$ ,  $Il-17A$  and  $Il-23$  were significantly reduced, indicating a limited therapeutic effect. Notably, the mRNA level of  $Il-23$ , which is mainly secreted from mature DCs, was significantly lower in the CEL-MAN-LP group than that in the CEL-LPs group (Fig. 7A). Furthermore, CEL-MAN-LPs showed a better effect on inhibition of the mRNA level of  $Il-17A$  which is the downstream cytokine of  $Il-23$ , compared with the CEL-LPs (Fig. 7B). The above results demonstrate that the CEL-MAN-LPs markedly mitigated the cytokine storm in the psoriatic skin lesion and showed better efficacy on inhibition of DCs-related inflammatory cytokines compared with other treatments *in vivo*.

### 3.9. IHC and IF staining

The IL-23/IL-17 inflammation axis plays a key role in the pathological process of psoriasis. IL-23 and IL-17, which are mainly secreted from inflammatory DCs and CD4 helper T 17 (Th17) cells, respectively, are effective cytokines in this axis for psoriatic skin lesions<sup>6</sup>. So we further evaluated the expression levels of IL-23 and IL-17 in the psoriasis site with the IHC test. The IHC staining results of IL-23 and IL-17 in the skin tissue are shown in Fig. 8. The dark brown spots are representative of positive IL-23 or IL-17 staining. The expression levels of IL-23 and IL-17 in the skin significantly increased after application of IMQ. CEL, CEL-LPs and CEL-MAN-LPs showed reduced levels of both inflammatory cytokines. As expected, consistent with the result of the PCR experiment, the staining intensity of IL-23 and IL-17 of the skin section in the CEL-MAN-LPs group was markedly lower than that in the CEL-LPs group. This result may be attributed to a superior ant-maturation effect of CEL-MAN-LPs on the DCs

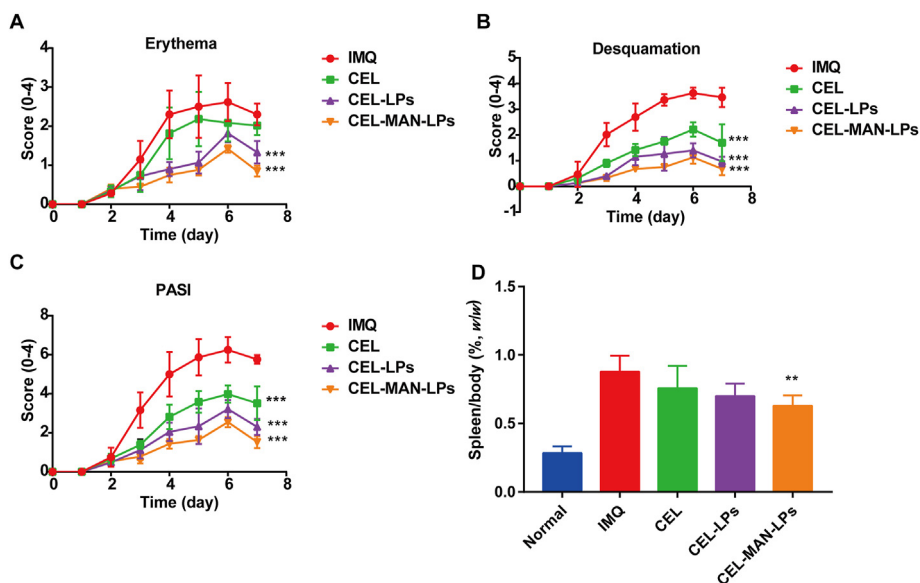


**Figure 6** The PASI scores including (A) erythema, (B) desquamation and (C) PASI total score of skin lesions after application of different treatment were recorded for 7 days, each score ranged from 0 to 4, and the total score from 0 to 8. (D) The spleen/body (% w/w) was recorded and calculated on Day 7. Data are presented as mean  $\pm$  SD ( $n = 6$ ),  $**P < 0.01$ ,  $***P < 0.001$ , compared with IMQ group.

which are the main effector cells in the IL-23/IL-17 inflammation axis. This conclusion was further proved in Section 3.10.

Ki67 is a cellular marker for proliferation and is highly expressed in the basal layer of the psoriatic epidermis, whereas normal basal cells barely express Ki67. As shown in Fig. 8, the expression levels of Ki67 protein in different mouse groups using IF staining were studied. The basal cells in the epidermis highly expressed the Ki67 protein (green) in the IMQ-induced group, while for the normal control group, only a few cells in the epidermis were marked with Ki67. After therapeutic treatment with CEL-LPs and CEL-MAN-LPs, Ki67 expression in the basal

layer markedly decreased, especially in the CEL-MAN-LPs group. The above results suggested that CEL-MAN-LPs showed the best inhibitory effect on epidermal cell hyperproliferation under psoriasis conditions.

### 3.10. The anti-maturation effect of CEL-MAN-LPs on DCs in lymphoid tissues

Mature DCs, which highly express MHC-II and costimulatory molecules such as CD80 and CD86, can interact with T cells and trigger the adaptive immune response in lymphoid tissues. To

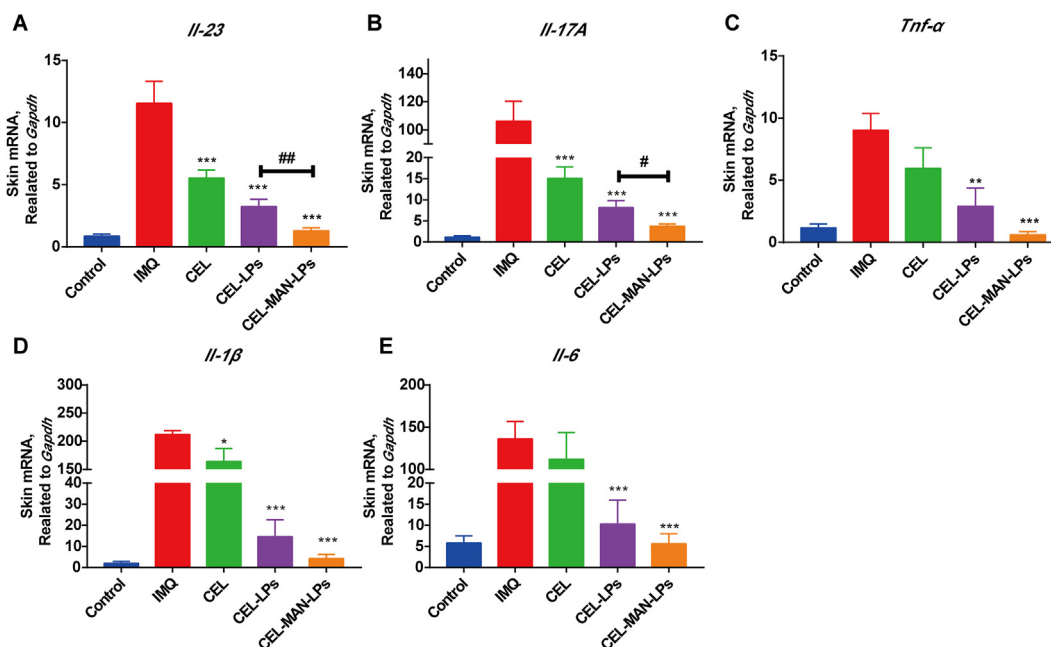


**Figure 7** The mRNA levels of inflammatory cytokines in the skin lesion treated with different preparations. (A) *Il-23*, (B) *Il-17A*, (C) *Tnf- $\alpha$* , (D) *Il-1 $\beta$* , (E) *Il-6*.  $*P < 0.05$ ,  $**P < 0.01$ ,  $***P < 0.001$  compared with IMQ group,  $#P < 0.05$ ,  $##P < 0.01$  compared with indicated group. Each value represents the mean and SE ( $n = 6$ ).

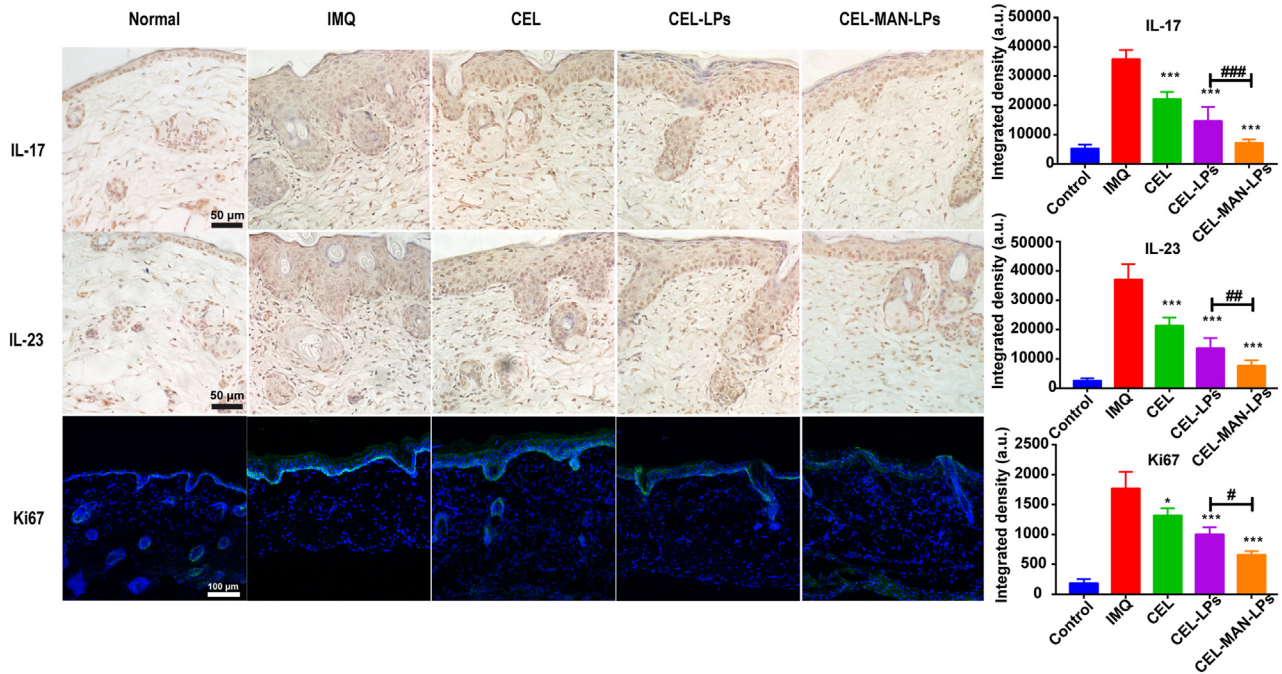


**Figure 8** The expression of IL-17 (IHC × 400), IL-23 (IHC × 400) and Ki67 (green, IF × 200) in the skin lesion after different treatment. \**P* < 0.05 and \*\*\**P* < 0.001 compared with IMQ group, #*P* < 0.05 ##*P* < 0.01 and ###*P* < 0.001 compared with indicated group. Each value represents the mean and SD (*n* = 3). Scale bar = 50 μm (IL-17 and IL-23), scale bar = 100 μm (Ki67).

further exploit the immune-regulatory mechanism of CEL-MAN-LPs in the psoriatic mouse model, we tested the maturation status of DCs in the DLNs and spleens from psoriatic mice after treatment with CEL preparations (Fig. 9). The expression

levels of CD80, CD86 and MHC-II on DCs in DLNs dramatically increased in the psoriasis model group compared with the normal control group. As expected, CEL preparations obviously diminished the expression of CD80, CD86 and MHC-II, but raw

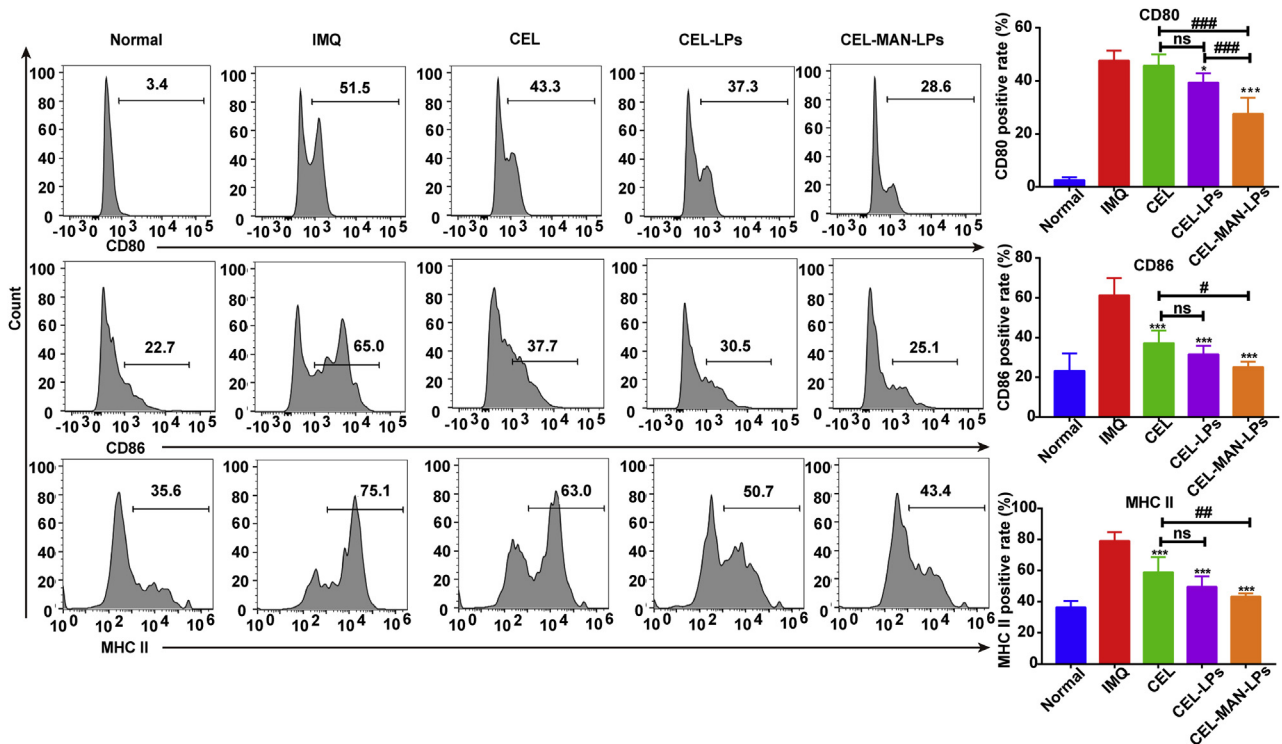


**Figure 9** The expression of maturation markers (CD80, CD86 and MHC-II) on the dendritic cells of DLN after receiving IMQ and different treatment for 6 days. Data are presented as mean ± SD (*n* = 6), \*\*\**P* < 0.001, compared with IMQ group. #*P* < 0.05, ##*P* < 0.01, ###*P* < 0.001, by comparison with the indicated group. ns, not significant.

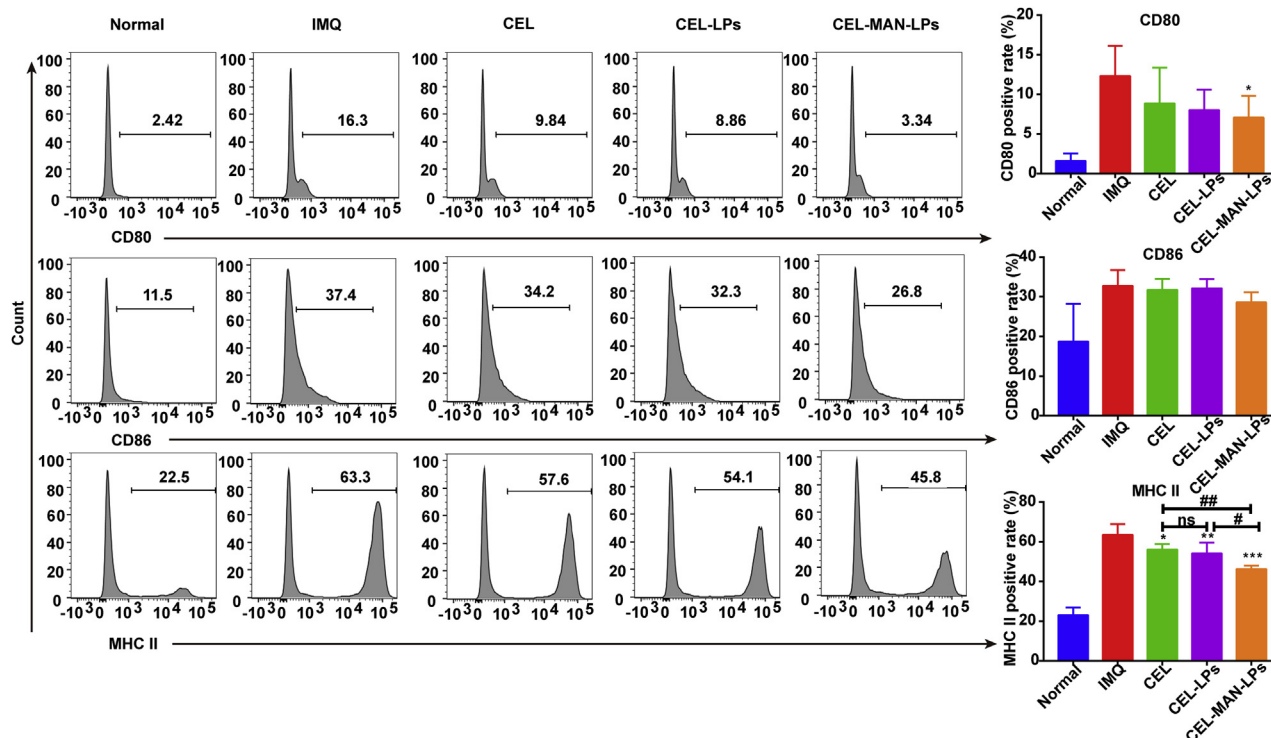


**Figure 10** The expression of maturation markers (CD80, CD86 and MHC-II) on the dendritic cells of spleen after receiving IMQ and different treatment for 6 days. Data are presented as mean  $\pm$  SD ( $n = 6$ ), \* $P < 0.05$ , \*\* $P < 0.01$ , \*\*\* $P < 0.001$ , compared with IMQ group. # $P < 0.05$ , ## $P < 0.01$ , by comparison with the indicated group. ns, not significant.

CEL only showed inhibition of the expression of CD86 and MHC-II, indicating limited anti-maturation ability. Notably, the inhibitory effect of CEL-MAN-LPs on the expression of CD80, CD86 and MHC-II was greatly enhanced compared with that of CEL.

In the assessment of the activation status of DCs in the spleen, all three DC maturation markers displayed significant upregulation in the psoriasis mouse model (Fig. 10). After treatment with CEL and CEL formulations, only the CEL-MAN-LPs significantly suppressed the expression of CD80 on splenic DCs. Although CEL-MAN-LPs showed a trend toward reduced CD86 expression, no significant difference was observed at the 0.05 level. In addition, the expression of MHC-II was significantly decreased after application of CEL and CEL preparations. Moreover, CEL-MAN-LPs exhibited a better inhibitory effect on MHC-II expression than CEL-LPs. Taken together, these results suggested that the anti-psoriasis efficacy may be attributable to the ability of CEL preparations to suppress the maturation of DCs, where the mannose modification strategy can enhance this anti-maturation ability of CEL on DCs *in vivo*.

### 3.11. Skin safety evaluation

The images of the healthy mouse skin which received injection of 0.9% saline, CEL solution (375  $\mu\text{g}/\text{kg}$ ), CEL-LPs or CEL-MAN-LPs with hollow microneedles for 6 days were shown in Supporting Information Fig. S6. The CEL and CEL preparations did not cause adverse reactions such as edema and erythema on the healthy mouse skin, indicating good skin safety of the treatment. Moreover, the microneedles which cause minimally invasive on the injection site are considered to be painless and have good patients' compliance<sup>43</sup>. Therefore, This treatment has good clinical potential.

## 4. Conclusions

In this study, we explored the bioactivity of CEL-MAN-LPs as a new CEL-loaded carrier for psoriasis treatment. The mannose modification strategy effectively enhanced DC uptake by fluorescence-labeled liposomes in both a cell model and a psoriatic mouse model. The CEL-MAN-LPs markedly improved the bioactivity of CEL by inhibiting the maturation of DCs both *in vitro* and *in vivo*. As a consequence, CEL-MAN-LPs showed superior efficacy in alleviating the psoriasis pathological symptoms and inhibiting the expression of the main inflammatory cytokines in psoriatic skin lesions compared with CEL and CEL-LPs. Moreover, the treatment exhibited good skin safety. In summary, the strategy to enhance DC uptake and induce DC tolerance by loading drugs *via* mannose-modified liposomes exhibited excellent anti-psoriasis activity, which has wide potential application in the treatment of other DC-associated types of inflammation in the future.

## Acknowledgments

This work was supported by research grants from the Macau Science and Technology Development Fund (0013/2018/A1, China) and a Research Grant from the University of Macau (MYRG2019-00032-ICMS, China). We thank the members of the FHS Animal Facility at the University of Macau for their experimental and technical support.

## Author contributions

Dr. Ying Zheng contributed to the design, discussion and writing of the manuscript. Mr. Long Xi carried out the experiments,

analyzed data and drafted the manuscript. Ms. Zibei Lin, Ms. Fen Qiu and Mr. Shaokui Chen participated part of the experiments. Dr. Zhenping Wang, Dr. Ping Li and Dr. Xin Chen offered suggestions on the experiment design. All of the authors have read and approved the final manuscript.

### Conflicts of interest

The authors have no conflicts of interest to declare.

### Appendix A. Supporting information

Supporting data to this article can be found online at <https://doi.org/10.1016/j.apsb.2021.07.019>.

### References

- Greb JE, Goldminz AM, Elder JT, Lebowitz MG, Gladman DD, Wu JJ, et al. Psoriasis. *Nat Rev Dis Primers* 2016;**2**:16082.
- Mabuchi T, Chang TW, Quinter S, Hwang ST. Chemokine receptors in the pathogenesis and therapy of psoriasis. *J Dermatol Sci* 2012;**65**: 4–11.
- Zachariae H, Zachariae R, Blomqvist K, Davidsson S, Molin L, Mørk C, et al. Quality of life and prevalence of arthritis reported by 5,795 members of the nordic psoriasis associations. *Acta Derm Venereol* 2002;**82**:108–13.
- Ahlehoff O, Skov L, Gislason G, Lindhardsen J, Kristensen SL, Iversen L, et al. Cardiovascular disease event rates in patients with severe psoriasis treated with systemic anti-inflammatory drugs: a Danish real-world cohort study. *J Intern Med* 2013;**273**:197–204.
- Sala M, Elaissari A, Fessi H. Advances in psoriasis physiopathology and treatments: up to date of mechanistic insights and perspectives of novel therapies based on innovative skin drug delivery systems (ISDDS). *J Control Release* 2016;**239**:182–202.
- Suzuki E, Mellins ED, Gershwin ME, Nestle FO, Adamopoulos IE. The IL-23/IL-17 axis in psoriatic arthritis. *Autoimmun Rev* 2014;**13**: 496–502.
- Nestle FO, Conrad C, Tun-Kyi A, Homey B, Gombert M, Boyman O, et al. Plasmacytoid dendritic cells initiate psoriasis through interferon- $\alpha$  production. *J Exp Med* 2005;**202**:135–43.
- Lowe M, Suárez-Farinas M, Krueger JG. Immunology of psoriasis. *Annu Rev Immunol* 2014;**32**:227–55.
- Singh TP, Zhang HH, Borek I, Wolf P, Hedrick MN, Singh SP, et al. Monocyte-derived inflammatory Langerhans cells and dermal dendritic cells mediate psoriasis-like inflammation. *Nat Commun* 2016;**7**: 1–18.
- Banchereau J, Briere F, Caux C, Davoust J, Lebecque S, Liu YJ, et al. Immunobiology of dendritic cells. *Annu Rev Immunol* 2000;**18**: 767–811.
- Wang MX, Zhao JX, Meng YJ, Di TT, Xu XL, Xie XJ, et al. Acetyl-11-keto-beta-boswellic acid inhibits the secretion of cytokines by dendritic cells via the TLR7/8 pathway in an imiquimod-induced psoriasis mouse model and *in vitro*. *Life Sci* 2018;**207**:90–104.
- Meng Y, Wang M, Xie X, Di T, Zhao J, Lin Y, et al. Paeonol ameliorates imiquimod-induced psoriasis-like skin lesions in BALB/c mice by inhibiting the maturation and activation of dendritic cells. *Int J Mol Med* 2017;**39**:1101–10.
- Qiu D, Kao PN. Immunosuppressive and anti-inflammatory mechanisms of triptolide, the principal active diterpenoid from the Chinese medicinal herb *Tripterygium wilfordii* Hook. f. *Drugs R D* 2003;**4**: 1–18.
- Wu C, Jin HZ, Shu D, Li F, He CX, Qiao J, et al. Efficacy and safety of *Tripterygium wilfordii* hook F versus acitretin in moderate to severe psoriasis vulgaris: a randomized clinical trial. *Chin Med J* 2015;**128**: 443.
- Venkatesha SH, Moudgil KD. Celastrol and its role in controlling chronic diseases. In: *Anti-inflammatory nutraceuticals and chronic diseases*. Cham: Springer; 2016. p. 267–89.
- Meng S, Sun L, Wang L, Lin Z, Liu Z, Xi L, et al. Loading of water-insoluble celastrol into niosome hydrogels for improved topical permeation and anti-psoriasis activity. *Colloids Surf B* 2019;**182**: 110352.
- Wang Y, Cao L, Xu LM, Cao FF, Peng B, Zhang X, et al. Celastrol ameliorates EAE induction by suppressing pathogenic T cell responses in the peripheral and central nervous systems. *J Neuroimmune Pharmacol* 2015;**10**:506–16.
- Boks MA, Ambrosini M, Bruijns SC, Kalay H, van Bloois L, Storm G, et al. MPLA incorporation into DC-targeting glycoliposomes favours anti-tumour T cell responses. *J Control Release* 2015;**216**:37–46.
- Barbosa JP, Neves AR, Silva AM, Barbosa MA, Reis MS, Santos SG. Nanostructured lipid carriers loaded with resveratrol modulate human dendritic cells. *Int J Nanomed* 2016;**11**:3501.
- Markov OV, Mironova NL, Shmendel EV, Serikov RN, Morozova NG, Maslov MA, et al. Multicomponent mannose-containing liposomes efficiently deliver RNA in murine immature dendritic cells and provide productive anti-tumour response in murine melanoma model. *J Control Release* 2015;**213**:45–56.
- Liang R, Xie J, Li J, Wang K, Liu L, Gao Y, et al. Liposomes-coated gold nanocages with antigens and adjuvants targeted delivery to dendritic cells for enhancing antitumor immune response. *Bio-materials* 2017;**149**:41–50.
- Qian Y, Jin H, Qiao S, Dai Y, Huang C, Lu L, et al. Targeting dendritic cells in lymph node with an antigen peptide-based nanovaccine for cancer immunotherapy. *Biomaterials* 2016;**98**:171–83.
- Tacke PJ, de Vries IJ, Torensma R, Figdor CG. Dendritic-cell immunotherapy: from *ex vivo* loading to *in vivo* targeting. *Nat Rev Immunol* 2007;**7**:790–802.
- Unger WW, van Kooyk Y. Dressed for success C-type lectin receptors for the delivery of glyco-vaccines to dendritic cells. *Curr Opin Immunol* 2011;**23**:131–7.
- Wijagkanalan W, Kawakami S, Higuchi Y, Yamashita F, Hashida M. Intratracheally instilled mannosylated cationic liposome/NFkappaB decoy complexes for effective prevention of LPS-induced lung inflammation. *J Control Release* 2011;**149**:42–50.
- Wijagkanalan W, Kawakami S, Takenaga M, Igarashi R, Yamashita F, Hashida M. Efficient targeting to alveolar macrophages by intratracheal administration of mannosylated liposomes in rats. *J Control Release* 2008;**125**:121–30.
- Kurian A, Barankin B. Current effective topical therapies in the management of psoriasis. *Skin Therapy Lett* 2011;**16**:4–7.
- Menter A, Korman NJ, Elmets CA, Feldman SR, Gelfand JM, Gordon KB, et al. Guidelines of care for the management of psoriasis and psoriatic arthritis: section 3. Guidelines of care for the management and treatment of psoriasis with topical therapies. *J Am Acad Dermatol* 2009;**60**:643–59.
- Sun L, Liu Z, Wang L, Cun D, Tong HH, Yan R, et al. Enhanced topical penetration, system exposure and anti-psoriasis activity of two particle-sized, curcumin-loaded PLGA nanoparticles in hydrogel. *J Control Release* 2017;**254**:44–54.
- An M, Liu H. Dissolving microneedle arrays for transdermal delivery of amphiphilic vaccines. *Small* 2017;**13**:1700164.
- Liu S, Jin MN, Quan YS, Kamiyama F, Katsumi H, Sakane T, et al. The development and characteristics of novel microneedle arrays fabricated from hyaluronic acid, and their application in the transdermal delivery of insulin. *J Control Release* 2012;**161**: 933–41.
- Li WZ, Huo MR, Zhou JP, Zhou YQ, Hao BH, Liu T, et al. Super-short solid silicon microneedles for transdermal drug delivery applications. *Int J Pharm* 2010;**389**:122–9.
- Jiang T, Wang T, Li T, Ma Y, Shen S, He B, et al. Enhanced transdermal drug delivery by transfersome-embedded oligopeptide hydrogel for topical chemotherapy of melanoma. *ACS Nano* 2018;**12**: 9693–701.

34. Tas C, Mansoor S, Kalluri H, Zarnitsyn VG, Choi SO, Banga AK, et al. Delivery of salmon calcitonin using a microneedle patch. *Int J Pharm* 2012;**423**:257–63.
35. Wang PM, Cornwell M, Hill J, Prausnitz MR. Precise microinjection into skin using hollow microneedles. *J Invest Dermatol* 2006;**126**: 1080–7.
36. Roxhed N, Samel B, Nordquist L, Griss P, Stemme G. Painless drug delivery through microneedle-based transdermal patches featuring active infusion. *IEEE Trans Biomed Eng* 2008;**55**:1063–71.
37. Dul M, Stefanidou M, Porta P, Serve J, O'Mahony C, Malissen B, et al. Hydrodynamic gene delivery in human skin using a hollow microneedle device. *J Control Release* 2017;**265**:120–31.
38. Alkilani AZ, McCrudden MT, Donnelly RF. Transdermal drug delivery: innovative pharmaceutical developments based on disruption of the barrier properties of the stratum corneum. *Pharmaceutics* 2015;**7**: 438–70.
39. Chen X, Hu X, Hu J, Qiu Z, Yuan M, Zheng G. Celastrol-loaded galactosylated liposomes effectively inhibit AKT/c-Met-triggered rapid hepatocarcinogenesis in mice. *Mol Pharm* 2020;**17**:738–47.
40. Zhang Y, Kim TJ, Wroblewska JA, Tesic V, Upadhyay V, Weichselbaum RR, et al. Type 3 innate lymphoid cell-derived lymphotoxin prevents microbiota-dependent inflammation. *Cell Mol Immunol* 2018;**15**:697–709.
41. Chen J, Son HN, Hill JJ, Srinivasan S, Su FY, Stayton PS, et al. Nanostructured glycopolymer augmented liposomes to elucidate carbohydrate-mediated targeting. *Nanomedicine* 2016;**12**:2031–41.
42. Ke X, Howard GP, Tang H, Cheng B, Saung MT, Santos JL, et al. Physical and chemical profiles of nanoparticles for lymphatic targeting. *Adv Drug Deliv Rev* 2019;**151–152**:72–93.
43. Zhu DD, Zhang XP, Zhang BL, Hao YY, Guo XD. Safety assessment of microneedle technology for transdermal drug delivery: a review. *Adv Ther* 2020;**3**:2000033.